Hindawi Publishing Corporation
Journal of Nanomaterials
Volume 2013, Article ID 136145, 9 pages
http://dx.doi.org/10.1155/2013/136145

Research Article

Synthesis of Nanosized Zinc-Doped Cobalt Oxyhydroxide Parties by a Dropping Method and Their Carbon Monoxide Gas Sensing Properties

Jian-Wen Wang and Yi-Ming Kuo

Department of Safety Health and Environmental Engineering, Chung Hwa University of Medical Technology, Tainan 717, Taiwan

Correspondence should be addressed to Jian-Wen Wang; jinwen.tw@yahoo.com.tw

Received 22 August 2012; Revised 21 December 2012; Accepted 23 December 2012

Academic Editor: Jinquan Wei

Two nanostructures of cobalt oxyhydroxide (CoOOH) and Zinc-(Zn-) doped CoOOH (1–4% Zn) are prepared from $Co(NO_3)_2$ solution via microtitration with NaOH and oxidation in air. The X-ray diffraction (XRD) analysis results show that a pure state of nano-CoOOH can be obtained at an alkalinity (OH^-/Co^+) of 5 with 40°C heat treatment after 6 h. The Zn ions preferentially substitute Co ions in the CoOOH structure, resulting in a decrease of its crystallinity. The disc-like CoOOH nanostructure exhibits good sensitivity to carbon monoxide (CO) in a temperature range of 40–110°C with maximum sensitivity to CO at around 70–80°C. When CoOOH nanostructure is doped with 1% Zn, its sensitivity and selectivity for CO gas are improved at 70–80°C; further Zn doping to 2% degraded the CO sensing properties of nano-CoOOH. The results of a cross-sensitivity investigation of the sensor to various gases coexisting at early stages of a fire show that the sensitivity of Zn-doped nano-CoOOH is the highest toward CO. Zn-doped nano-CoOOH film exhibits a high sensitivity to CO at room temperature, making it a promising sensor for early-stage fire detection.

1. Introduction

Fire detection systems are designed to respond to the smoke, heat, and electromagnetic radiation generated during smoldering and flaming combustion. It is known that decomposed gases, which are emitted in the preliminary stage of a fire, are generated before smoke. Therefore, numerous studies have developed gas sensors for fire detection [1]. Based on European standard EN 54, CO is a major by-product at early stages of a fire for all 6 typical fire scenarios [2]. Highly sensitive CO sensors can provide early fire detection and reduce false alarm rates [3].

Early fire detection requires that all major by-products of complete and/or incomplete combustion (including CO) should be detected rapidly in a relatively low temperature range of 60–100°C (i.e., when a fire has just started). Several semiconducting metal oxides have been used in CO gas sensors, including SnO_2, ZnO, Fe_2O_3, $BaTiO_3$, TiO_2, In_2O_3, and Zn_2SnO_4 [4]. However, these CO gas sensors require relatively high operating temperatures (above 400°C) [5–7]. Therefore, CO gas sensors that operate at a relatively low temperature are desirable.

CoOOH (cobalt oxyhydroxide), a high-conductivity active material used in conjunction with nickel hydroxide in Ni–H cells, has been proposed as an alternative material for CO detection at low temperatures [8]. In contrast to Co_3O_4, CoOOH is a nonstoichiometric oxide; Co has a higher oxidation state (+3) than that of Co_3O_4 (+2). Some studies on the oxidation of CO [9, 10] have shown that cobalt Co (+3) ions are active in the reaction. Results revealed that although response and recovery rates at low temperatures are an issue, the temperature for the maximum CO sensitivity level for CoOOH could be decreased down to 80°C [11].

Many approaches have been proposed for modifying the sensing properties of semiconductor oxide CO sensors to achieve high sensitivity and selectivity. Grain size reduction

is another approach to enhancing gas sensitivity. Zhuiykov and Dowling [12] showed that dumbbell-like CoOOH nanostructures exhibit high sensitivity to CO at room temperature as well as good reproducibility and short response/recovery times. The gas sensitivity is expected to increase when the grain size becomes smaller than the space charge depth [13]. Thus, in this study, nanosized CoOOH was synthesized by a modified dropping method using a peristaltic pump to avoid excessive volume of sodium hydroxide solution drop into cobalt nitrate solution resulting in the rapid growth of precursor particles.

Noble metals (Ag, Au, Pt, and Pd) are well known for enhancing the rate of response and increasing selectivity to a single gas. Shimizu and Egashira [14] indicated that CO sensitivity and selectivity of a nanostructured CoOOH CO sensor can be increased by Au nanoparticle addition. The results also showed that Au nanoparticles enhance the reaction kinetics at low temperature. In addition, Bahlawane et al. [15] indicated that the addition of nickel or zinc affects the conductivity of Co_3O_4, generating metal vacancies and decreasing resistivity. Similar results for the addition of SnO_2 to Co_3O_4 sensor materials were reported [16]. SnO_2 addition to Co_3O_4 leads to an increase in sensor resistance compared to that of undoped Co_3O_4. Thus, it was considered that similar promotion effects can be obtained for nano-CoOOH doped by Zn or Ni. Therefore, we attempted to further improve the CO sensing properties by the development of a nanostructure of CoOOH doped with Zn in this study.

2. Experimental Procedure

2.1. Sample Preparation. In a typical synthesis of CoOOH nanomaterials, 100 mL of 2.5 M NaOH solution was added dropwise into 100 mL of 0.5 M cobalt nitrate ($Co(NO_3)_2{\cdot}6H_2O$) solution with a peristaltic pump to form a $Co(OH)_2$ precursor. The pH value was kept below 9 during the mixing process. The red color of $Co(NO_3)_2{\cdot}6H_2O$ gradually changed to deep blue and finally to pink. When the pH was increased to $9 < pH < 14$, the color of the $Co(OH)_2$ precipitate turned brown with the formation $Co(OH)_3{\cdot}$CoOOH was obtained from $Co(OH)_3$ by holding in 40°C water bath for 1~6 hr. The final brown precipitate was filtered and washed with deionized water three times, then dried at 60°C for 2 days, and collected as CoOOH.

CoOOH nanopowders doped with Zn were synthesized by a hydrothermal method. Some of the CoOOH nanopowders were ultrasonically dispersed into methanol (200 mL) at about 60°C. Subsequently, 0.01 M $Zn(Ac)_2$ was dissolved into the above solution. Then, a 0.03 M solution of KOH (65 mL) in methanol was added dropwise. The reaction mixture was stirred for 2 h. The resulting solution was concentrated by the evaporation of the solvent. The resulting white product was centrifuged and then washed with deionized water and ethanol to remove any remaining ions in the final product. The CoOOH nanopowders doped with Zn of Zn : Co molar ratios of 0, 1, 2, 3, and 4% were prepared.

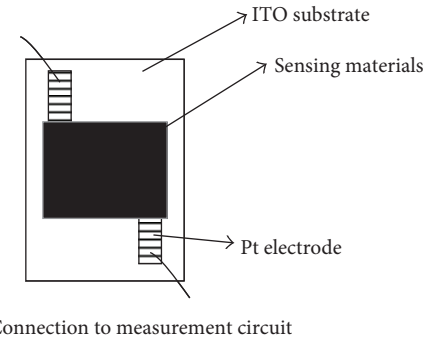

Figure 1: Structure of sensing element.

2.2. Sample Characterization. Thermogravimetric/differential thermal analysis (TG/DTA) of the CoOOH-based nanostructure was conducted using a differential thermal analyzer (Setaram Setsys Evolution 1600, France). A gas flow rate of 100 cm^3/min was maintained for all experiments. The temperature was increased at a rate of 10°C/min from room temperature up to 1000°C.

The crystalline phase was identified using an X-ray diffractometer (XRD, Model Rad IIA, Rigaku Co., Tokyo, Japan) with Cu Kα radiation and an Ni filter, operated at 30 kV, 20 mA, and a scanning rate of 4°/min. The surface morphology of the CoOOH-based powders was examined by a field-emission scanning electron microscope (FE-SEM, XL-40 FEG SEM, Philips, Eindhoven, Holland).

2.3. Gas Sensing Experiments. Sensing material was prepared in the form of a paste by mixing an appropriate amount of glycerol, 3 g CoOOH or Zn-doped CoOOH powder, and 1mL tetraethyl orthosilicate (TEOS) binder. Nanostructured layers of Zn-doped CoOOH and pure CoOOH were deposited onto indium tin oxide (ITO) substrates between attached Pt electrodes by using an organic binder. Figure 1 shows the structure of the sensing element.

Gas sensing experiments were carried out in a self-designed conventional flow apparatus equipped with heating facility. Each sensor was exposed to a constant flow of dry air (100 cm^3/min) or a sample gas (CO or other calibrated gases in dry air), while the electrical resistance of the sensor was monitored by an Agilent 34970A multimeter, which was connected to a PC. The sensor responses was defined as $S = Rg/Ra$ for pure CoOOH and Zn-doped CoOOH nanostructures, where Rg and Ra denote the sensor electrical resistance in a sample gas and in air, respectively. Measurements were performed between room temperature and 100°C with CO content of 100 ppm. The temperature was carefully measured using a K-type thermocouple located adjacent to the CO sensor. The cross-sensitivity of the cobalt oxyhydroxide-based sensors to various gaseous pollutants that are usually by-products of fires was examined. A 100 ppm concentration was chosen for all gases that included CO, except carbon dioxide.

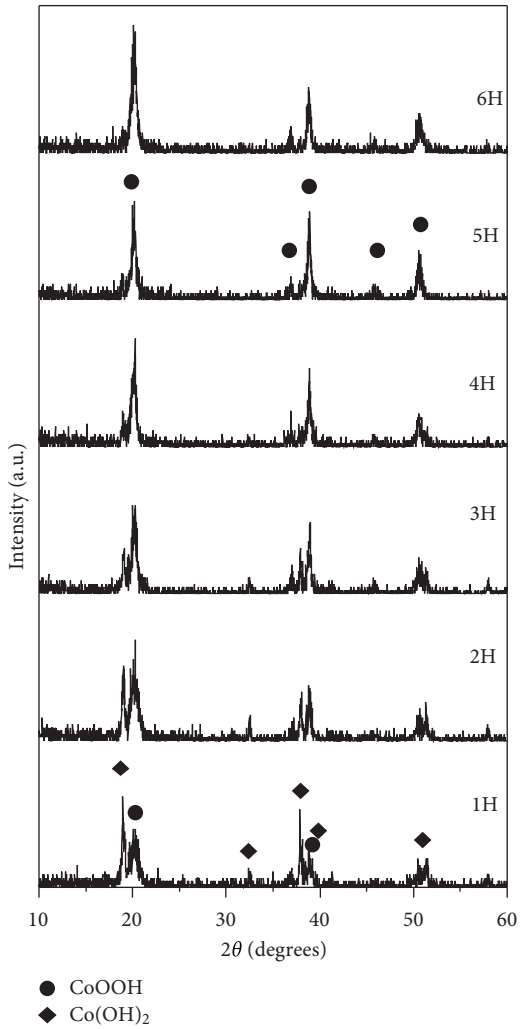

Figure 2: XRD patterns of cobalt oxide samples that underwent hydrothermal treatment at 40°C for various holding times.

3. Results and Discussion

3.1. Characterization of Nano-CoOOH. Figure 2 shows XRD patterns of cobalt oxide samples that underwent hydrothermal treatment at 40°C for various holding times. The main peaks were attributed to the $Co(OH)_2$ structure after one hour. With increasing retention time, the peaks intensity of the $Co(OH)_2$ structure decreased and then gradually transformed into those of the CoOOH phase. A pure phase of nanosized CoOOH can be obtained with a retention time of 5 h or longer. The results were verified by JCPD cards (JCPDC 14-0673).

Figures 3(a) and 3(b) show the morphology of CoOOH precursors and nanosized CoOOH prepared by hydrothermal treatment at 40°C for 6 h, respectively. Figure 3(a) shows that the initial compound is composed of many nanoparticles that were created during the titration reaction. Since the surface energy of nanomaterials tends to aggregate in large particles, CoOOH precursors aggregated into an irregular plated form; the plate size was 50–150 nm in length and 30–40 nm in width. However, some rod-like structures were scattered all over the corner region. They may be CoOOH nanostructures in a linear plated form. After hydrothermal treatment, $Co(OH)_3$ transformed into a CoOOH structure. The surface morphology is shown in Figure 3(b). The OH functional groups were removed by the heating process, resulting in the irregular plate structure transforming into a disc-like structure. The particle size was 100–150 nm in diameter. The crystalline grain boundaries became obvious. The nanostructure increased the powder surface area and enhanced the sensitivity of the gas sensor.

Figure 4 shows TG/DTA measurements of nano-CoOOH in air. TGA data illustrate that after the initial loss of moisture, accumulated in the nanostructured CoOOH, the loss of weight from 200 to 400°C was due to a gradual decomposition of CoOOH. Co_3O_4 formed via the decomposition of CoOOH, with O_2 and H_2O also produced, when the temperature was above 300°C. Reaction (1) is an exothermic process, as confirmed by DTA analysis

$$12\mathrm{CoOOH} \longrightarrow 4\mathrm{Co_3O_4} + \mathrm{O_2} + 6\mathrm{H_2O} \quad (1)$$

Co_3O_4 was converted into CoO and O_2 after a further increase of temperature via the following endothermic reaction:

$$2\mathrm{Co_3O_4} \longrightarrow 6\mathrm{CoO} + \mathrm{O_2} \quad (2)$$

Reaction (2) is endothermic. Co_3O_4 is thermodynamically more stable than CoO. The weight losses in reactions (1) and (2) are 10.36% and 6.1%, respectively. The results obtained experimentally are in good agreement with the calculated values of 12.7% and 6.6%, respectively.

3.2. Characterization of Zn-Doped Nano-CoOOH. Figure 5 shows XRD patterns as a function of the Zn doping amount in the nano-CoOOH lattice. The refraction peaks of CoOOH can be indexed to a rhombohedral structure. As the amount of Zn^{2+} increases, the characteristic peak intensity of CoOOH decreases and additional peaks appear. The positions of the main diffraction peaks evidently shift to the smaller angle side with the increasing zinc content. This shift of diffraction angles indicates that Zn^{2+} ions have been successfully doped into the crystal lattice of CoOOH host. These phenomena can be explained in terms of the larger covalent radius of Zn^{2+} (0.74 Å) than that of Co^{3+} (0.63 Å). The Zn^{2+} ions doped into the CoOOH matrix necessarily results in the expansion of the unit-cell volume of the Zn-doped CoOOH nanocrystals owing to the larger covalent radius of Zn^{2+} ions. In addition, the (003) peak exhibits significant broadening, which may be attributed to the disorder in the (003) side of Zn-doped CoOOH nanocrystals. When the amount of Zn^{2+} was higher than 2%, the characteristic peak (003) of CoOOH disappeared. This indicates that some Zn^{2+} did not enter the crystal lattice of CoOOH, forming a ZnO structure. For Zn^{2+} doping amounts higher than 2%, the crystallinity of ZnO increased. The changes in the structure from CoOOH to ZnO are not favorable for CO detection at low temperatures, as confirmed by electrical conductivity results of the materials.

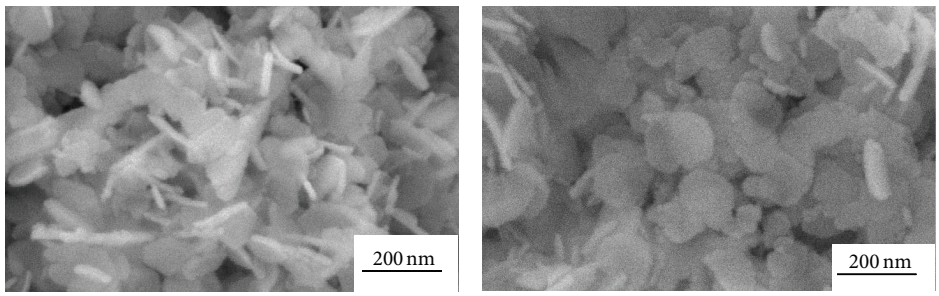

Figure 3: Morphology of (a) CoOOH precursors and (b) nanosized CoOOH prepared by hydrothermal treatment at 40°C for 6 h.

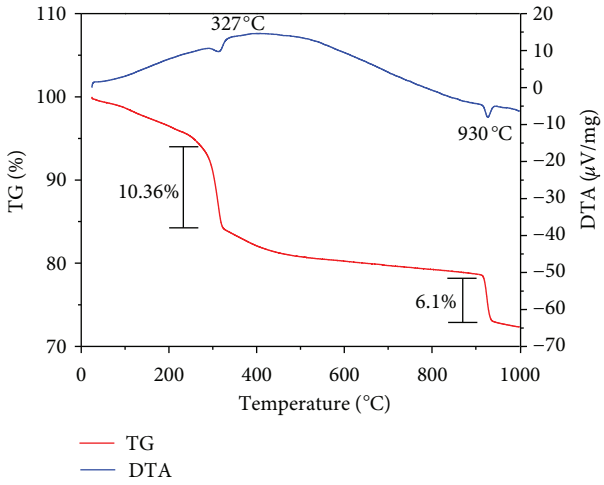

Figure 4: TG/DTA curves of the nano-CoOOH in air.

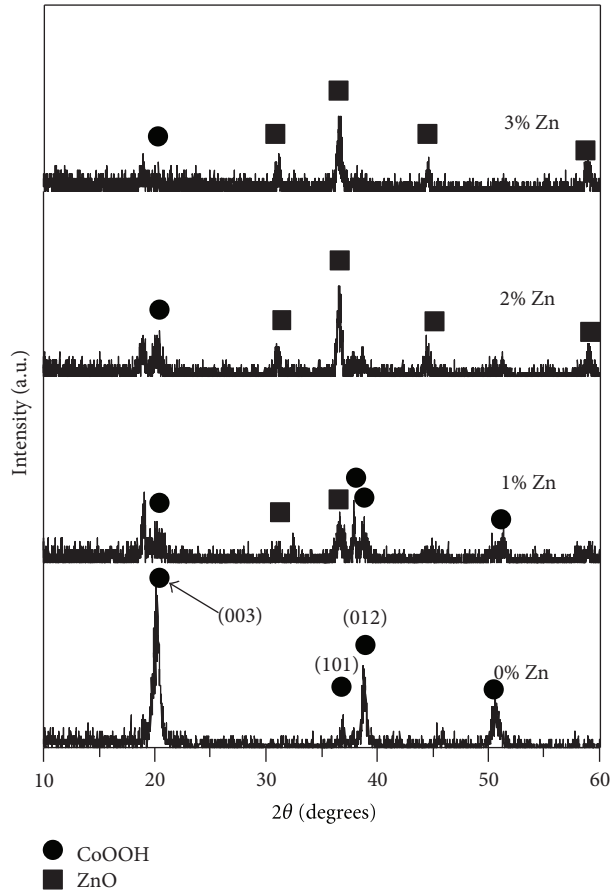

Figure 5: XRD patterns as a function of Zn doping amount in nano-CoOOH lattice.

Figure 6 shows the surface morphology of nano-CoOOH with various Zn doping amounts. The plate and disc-like structures of nano-CoOOH gradually transformed into spherical particles as the Zn doping amount increased from 1% to 2%. When the Zn amount was increased to 3%, the nanoparticle size decreased to 30–40 nm in diameter. However, the nanoparticles tended to aggregate and the particle size increased with the Zn doping amount for concentrations above 4%. Some necking structures were found between particles. Added impurities may influence the size and morphology of a given crystal by participating in the nucleation and growth, in which many overall factors integrate to dominate the process. Meanwhile, the real behavior of crystal growth in nanocrystalline semiconductors may vary between fractal aggregation in the inauguration period and the subsequent diffusion process [17]. Change in morphology would be affected by the nucleation and growth process that would depend upon the above parameters as well as the charge status of the surface states and the dangling bonds. Compared to undoped sample, doped CoOOH nanocrystals shows individual grains clearly and its average particle size shrinks with different impurities.

Figure 7(a) shows TGA measurements of Zn-doped nano-CoOOH in air. The nanocomplex in the range of 200–400°C was the decomposition behavior similar to that of nano-CoOOH. It gradually lost its weight (6%) when the Zn doping amount was 1%. However, the weight loss of the nanocomplex significantly decreased (2% and 0.3%) when the Zn doping amount was increased to 2% and 3%. XRD analysis results confirm that Zn^{2+} doped into the crystal lattice CoOOH host, resulting in a significantly reduced amount of nano-CoOOH decomposition. Figure 7(b) shows that the exothermic peak (327°C) tended to decrease as the Zn doping amount increased. This indicates that the reaction that

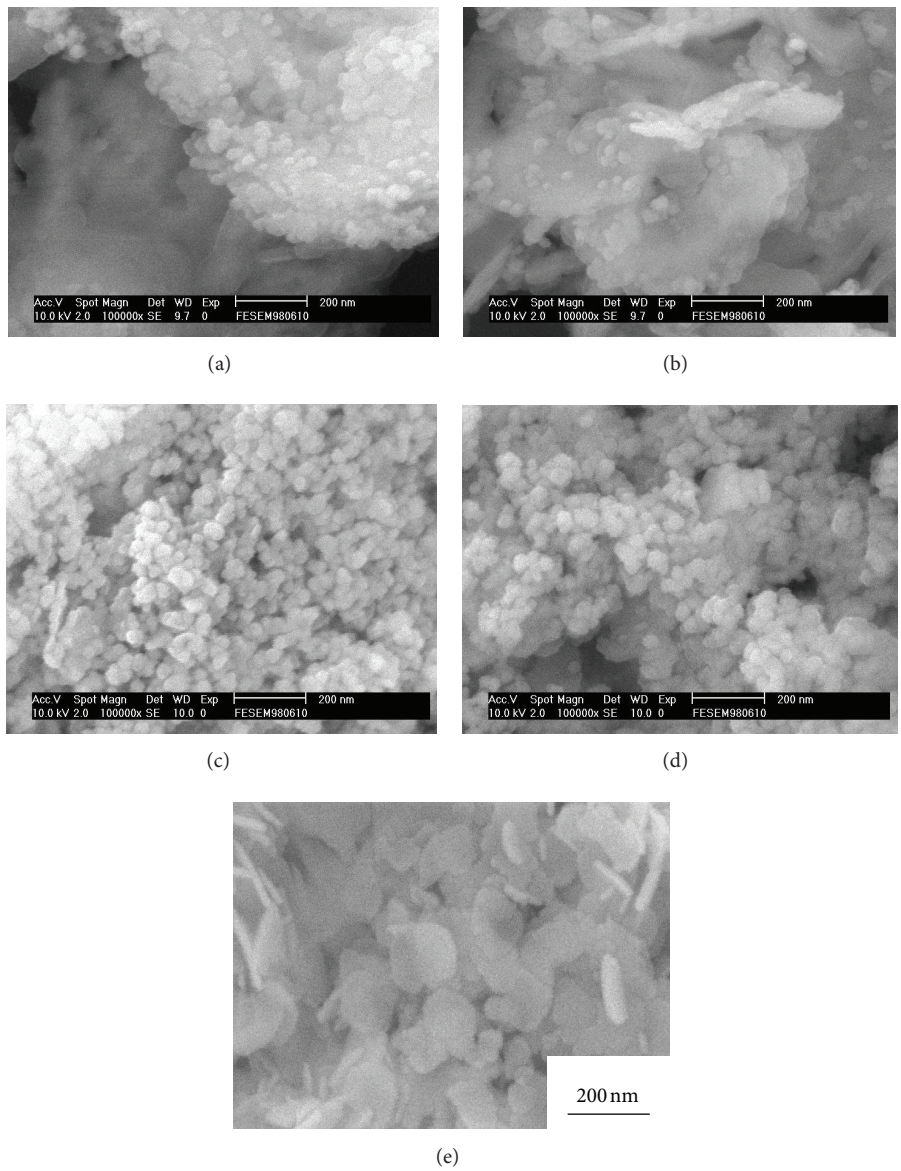

Figure 6: Surface morphologies of nano-CoOOH with Zn doping concentrations of (a) 1%, (b) 2%, (c) 3%, (d) 4%, and (e) 0%.

transformed some CoOOH into Co_3O_4 gradually decreased as the Zn doping amount was increased. Moreover, during the first stage of 200–400°C, there is weight loss about 6% to 0.3%, indicating the formation of $Zn_xCo_{3-x}O_4$ nanocomplex. The sharp weight loss at 930°C has been confirmed the complete decomposition of nanocomplex structure into ZnO and CoO [18]. The CoOOH structure was disrupted when the Zn doping amount was above 2%, resulting in a decrease of high-activity reaction areas of nano-CoOOH.

According to the results of XRD, SEM, and TGA/DTA, the Zn doping amount was set to below 3% for subsequent CO sensing tests.

3.3. Sensing Properties of Nano-CoOOH and Zn-Doped Nano-CoOOH. Figure 8 shows the electrical resistance of nano-CoOOH and Zn-doped nano-CoOOH in air as a function of temperature in the range of 40–100°C. The resistance of CoOOH increased with temperature in the range of 40 to 70°C. However, the resistance of CoOOH decreased with temperature for temperatures over 70°C. CoOOH can be regarded as a p-type semiconductor [19]. Therefore, the free electrons in CoOOH should become more active as the temperature increases, resulting in a decrease in the resistance of CoOOH. However, the resistance of CoOOH increased with temperature in the range of 40 to 70°C. According to Tobias et al. [20], CoOOH has a layered structure, and the high electrocatalytic activity of the inner sphere reactions on oxide materials is associated with surface defects. Active surface sites are found on step edges and corners of CoOOH. In the range of 40–70°C, the heat was insufficient to cause electron hopping in the layered structure, resulting in a conductive behavior of the metal oxide. However, when the

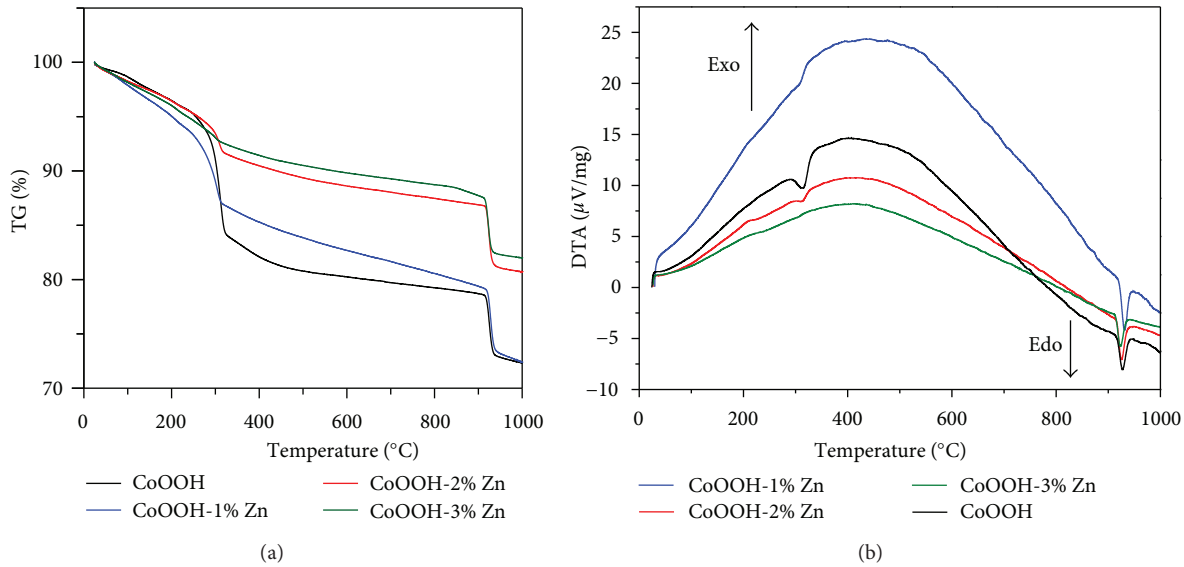

Figure 7: TGA/DTA curves of Zn-doped nano-CoOOH in air.

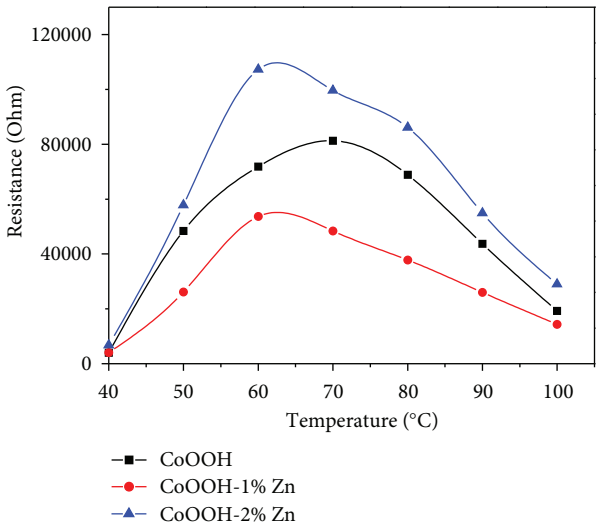

Figure 8: Electrical resistance of nano-CoOOH and Zn-doped nano-CoOOH in air as a function of temperature in the range of 40–100°C.

temperature was above 70°C, the electrons hopped between the surface defects of CoOOH, resulting in a decreased resistance. This behavior is similar to the semiconductor conduction mechanism.

Figure 8 also shows that the resistance of nano-CoOOH decreased with temperature when the Zn doping amount was increased to 1% in the range of 40 to 100°C. However, the resistance of nano-CoOOH increased with temperature when the Zn doping amount was over 1%. This indicates that appropriate zinc ion addition can reduce the resistance of nano-CoOOH. In addition, a low doping amount of zinc ions results in a small change in resistance with temperature. However, a rapid increase in resistance with temperature in the range of 60–70°C was found when the Zn doping amount was over 1%. Excess zinc oxide formed in the CoOOH structure for a high Zn doping amount. Therefore, the electron hopping in the metal oxide was easily blocked, resulting in higher resistance. XRD analysis results confirm that the addition of zinc ions resulted in some structural distortion in CoOOH. Hence, the conductivity of Zn-doped CoOOH decreased with temperature in the range of 40 to 60°C.

Figure 9 shows the sensor response to 1000 ppm CO in air for CoOOH and Zn-doped nano-CoOOH as a function of temperature. CoOOH exhibited a larger response (S = 6.87) over the temperature range of 70–80°C. The CO sensing mechanism of CoOOH has been proposed to take the form of gas-phase CO adsorption and desorption at active sites on the nano-CoOOH surface and the form of a surface oxidation reaction between adsorbed CO and adsorbed oxygen atoms (O^-) [21]. The surface oxidation reaction of CO^- with O^- produces CO_2 (3). Therefore, the active vacant sites on the CoOOH surface decrease, resulting in a decreased conductivity

$$CO + O^- \longrightarrow CO_2 + e^- \quad (3)$$

However, when the temperature exceeded 70°C, the sensitivity of nano-CoOOH decreased with temperature. CO adsorption is an exothermic reaction, so it is unfavorable to proceed when the temperature exceeds a certain critical point. Therefore, the best operating temperature of nano-CoOOH is 70–80°C for CO detection. Figure 9 also shows that the CO sensitivity of Zn-doped nano-CoOOH-based devices initially increases with temperature, with maximum values (S = 7.88) at around 70°C. The results presented in Figure 9 are consistent with similar results recently obtained by Wu et al. [22] and Zhuiykov [23]. However, the magnitude of the sensor response to 1000 ppm CO for the nano-CoOOH and 1% Zn-doped nano-CoOOH-based device was

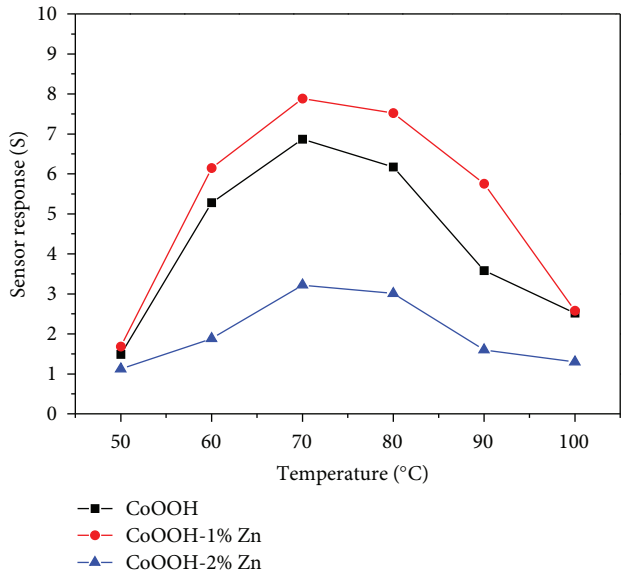

Figure 9: Sensor response to 1000 ppm CO in air for nano-CoOOH and Zn-doped nano-CoOOH as a function of temperature.

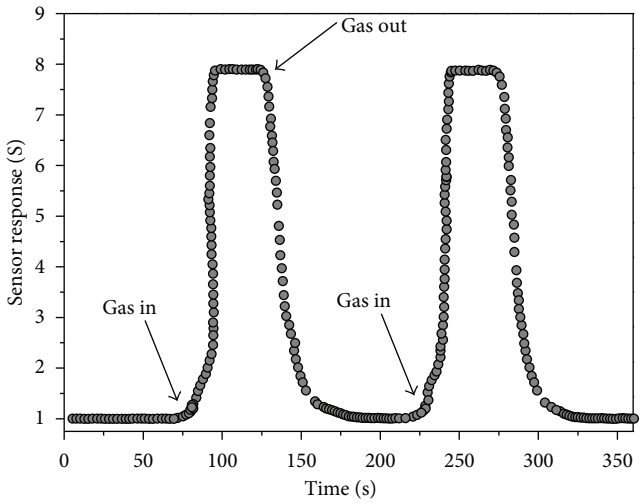

Figure 10: Response transients of 1% Zn-doped nano-CoOOH to 100 ppm CO at 70°C.

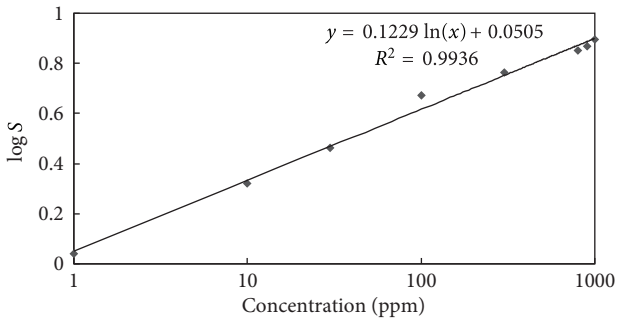

Figure 11: CO calibration curve of 1% Zn-doped nano-CoOOH sensor.

greater than that for those CoOOH thin-film screen-printed on the alumina substrate. This is probably due to a much higher surface-to-volume ratio provided by nanotechnology [12]. For Zn-doped nano-CoOOH, the maximum sensor response was obtained for the device doped with 1% Zn. 2% Zn doping degraded the CO sensitivity substantially. The results obtained during this investigation agree with published results for an H_2 sensor based on Co-doped SnO_2 nanofibers [24]. With excess Zn content, the p-type characteristics of CoOOH regress, and the p-type response decreases accordingly. This indicates that Zn promotes the sensor response to CO until its content in the nanostructure exceeds a critical value.

The response and recovery time of sensors based on 1% Zn-doped nano-CoOOH were investigated for different CO concentrations at a measuring temperature of 70°C as Figure 10 show. The sensor response changed rapidly from the base level upon switching to the different CO concentrations. The steady-state repeatable measuring values were attained at each measuring cycle. Typically, the 90% response and recovery times to 1000 ppm CO at an operating temperature of 70°C were 20 and 45 s, respectively. A low working temperature of 70°C combined with high CO sensitivity of 1% Zn-doped nano-CoOOH as well as good response and recovery rate is very attractive for using cobalt oxyhydroxide as a sensor material for semiconductor CO sensors. The promoting effects of Zn in the present sensors are likely to be associated with the enhancement of the conductivity of CoOOH nanostructures. Figure 11 shows response changes as the CO concentration varies from 1 to 1000 ppm. It was revealed that the linearity of the line formed by plotting log S against log [CO] was $R^2 = 0.9936$. The main effects of doping in CoOOH nanoparticles are the change in electronic conductivity and the introduction of defects into the nanoparticles. These factors play an important role to enhance the sensitivity in nanoparticles sensors. Defects within the crystal structure can improve the adsorption of gas molecules on the nanoparticle surface and the change in the conductivity will change the position of Fermi level in the energy band diagram which governs the electronic transportation between gas molecule and nanoparticle material [25]. In addition, the electrical detection of any chemical species is dependent on the surface reactions between the nanoparticles and the chemical molecules. Since the amount of Zn insertion into the nanoparticles was found to be small (1%), it is unlikely that solely chemical affinity can lead to the significant CO gas detection enhancement. Consequently, the interference effect experiments were carried out using for sensors based on 1% Zn-doped nano-CoOOH.

3.4. Interference Effect of Nano-CoOOH and Zn-Doped Nano-CoOOH. The cross-sensitivity of CO sensors based on nano-CoOOH and 1% Zn-doped nano-CoOOH to various co-existing gases was investigated. The gases and method were chosen as described in the French Standard [26] because they are applicable to studies and investigations on the fire behavior of substances and materials. The sensor response to the gases was tested in addition to the sensor response to

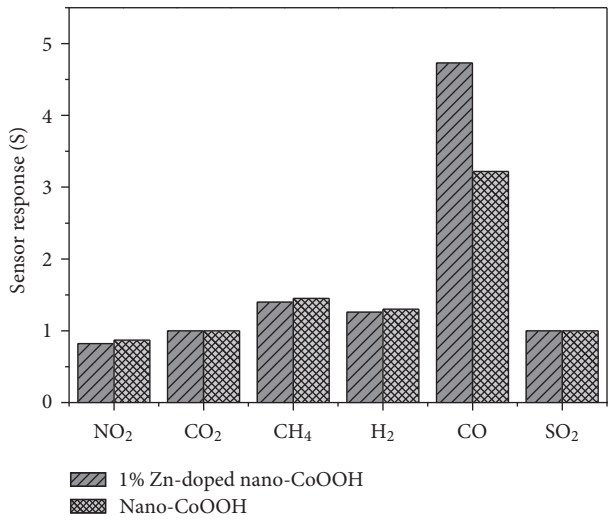

Figure 12: Cross-sensitivity of nano-CoOOH and 1% Zn-doped nano-CoOOH sensors to gases typically found at early stages of a fire.

the coexisting gases (NO_2, CO_2, CH_4, H_2, and SO_2) typical for various fire scenarios. Figure 12 shows that sensors using CoOOH have a maximum response ($S = 3.2$) near 70°C. At that temperature, the gases NO_2, CO_2, CH_4, H_2, and SO_2 (all 100 ppm) exhibit low interference with CO gas in a nano-CoOOH sensor. The figure also shows that the relative response to CO and H_2 (S_{CO}/S_{H_2}) of nano-CoOOH is near 2.5 (2.46) at 70°C. Therefore, the nanostructures enhance the sensitivity and selectivity of the reaction. Figure 9 also shows that sensors using Zn-doped CoOOH have a maximum response ($S = 4.73$) near 70°C. Furthermore, the relative response to CO and H_2 (S_{CO}/S_{H_2}) of Zn-doped CoOOH is near to 4 (3.64). It seems that the addition of zinc ions can effectively increase the sensitivity and selectivity for the CO gas. According to Potyrailo et al. [27], different parts of the nanoscales can affect the overall measurement upon interaction with different types of gaseous molecules, producing remarkably diverse and distinct differential reactions in real fire situations. Therefore, obtaining the required scale of the CoOOH is the keyto achieving a highly selective response to individual gaseous molecules.

4. Conclusion

CoOOH-based nanocomplexes were prepared from a $Co(NO_3)_2$ solution via a modified dropping method with NaOH and oxidation in air. The optimum working temperature of the CoOOH material for CO detection was roughly 70°C ($S = 6.87$). Zn doping enhanced the CO sensitivity of the CO sensor based on nano-CoOOH. Zn doping concentrations of 1% to 2% improved the reaction mechanism at a low temperature. Zn-doped nano-CoOOH exhibited a higher CO response than that of nano-CoOOH. The optimal CO sensing was obtained when the sensor was operated at 70°C, at which the sample exhibited a large response ($S = 7.88$) to 100 ppm CO. The Zn-doped nano-CoOOH also exhibited a high selectivity for CO relative to H_2 ($S_{CO}/S_{H_2} \sim 4$) in the CO concentration of 100 ppm. Zn-doped nano-CoOOH film exhibits high sensitivity and selectively to CO at room temperature, making it suitable for early fire detection.

Acknowledgment

The authors acknowledge the National Science Council of Taiwan, for financial support under Grant NSC 101-2221-E-273-003-MY2.

References

[1] Y. Watabe, T. Hujioka, N. Yamaga et al., "Application of micro-electrochemical CO sensor using solid electrolyte to fire detection," in *Digest of the 15th Chemical Sensor Symposium B*, vol. 8, pp. 53–56, 1992.

[2] EN 54 Standard, *Fire Detection and Fire Alarm Systems, Part 7*, British Standards Institute, 2001.

[3] B. C. Hagen and J. A. Milke, "Use of gaseous fire signatures as a mean to detect fires," *Fire Safety Journal*, vol. 34, no. 1, pp. 55–67, 2000.

[4] J. H. Du, R. C. Zhang, X. Y. Huang, X. Gong, and X. H. Zhang, "Research on early fire detection with CO-CO_2 FTIR-spectroscopy," *Spectroscopy and Spectral Analysis*, vol. 27, no. 5, pp. 899–903, 2007.

[5] J. H. Sung, Y. S. Lee, J. W. Lim, Y. H. Hong, and D. D. Lee, "Sensing characteristics of tin dioxide/gold sensor prepared by coprecipitation method," *Sensors and Actuators, B*, vol. 66, no. 1–3, pp. 149–152, 2000.

[6] P. Nellia, U. G. Fagliaa, G. Sberveglieria et al., "The aging effect on SnO_2-Au thin film sensors: electrical and structural characterization," *Thin Solid Films*, vol. 371, no. 1-2, pp. 249–253, 2000.

[7] K. Fukui and S. Nishida, "A theoretical treatment of molecular complexes i silver-aromatic hydrocarbon complexes," *Bulletin of the Chemical Society of Japan*, vol. 34, pp. 1076–1080, 1961.

[8] W. K. Hu, X. P. Gao, M. M. Geng, Z. X. Gong, and D. Noréus, "Synthesis of CoOOH nanorods and application as coating materials of nickel hydroxide for high temperature Ni-MH cells," *Journal of Physical Chemistry B*, vol. 109, no. 12, pp. 5392–5394, 2005.

[9] J. Jansson, A. E. C. Palmqvist, E. Fridell et al., "On the catalytic activity of Co_3O_4 in low-temperature CO oxidation," *Journal of Catalysis*, vol. 211, no. 2, pp. 387–397, 2002.

[10] F. Grillo, M. M. Natile, and A. Glisenti, "Low temperature oxidation of carbon monoxide: the influence of water and oxygen on the reactivity of a Co_3O_4 powder surface," *Applied Catalysis B*, vol. 48, no. 4, pp. 267–274, 2004.

[11] S. Mountford, "A sprinkler in the works," *Fire Prevention*, no. 366, pp. 48–49, 2003.

[12] S. Zhuiykov and V. Dowling, "The nanostructured Au-doped cobalt oxyhydroxide based carbon monoxide sensor for fire detection at its earlier stages," *Measurement Science and Technology*, vol. 19, no. 2, Article ID 024001, 2008.

[13] B. Geng, F. Zhan, H. Jiang, Z. Xing, and C. Fang, "Facile production of self-assembly hierarchical dumbbell-like CoOOH nanostructures and their room-temperature CO-gas-sensing properties," *Crystal Growth and Design*, vol. 8, no. 10, pp. 3497–3500, 2008.

[14] Y. Shimizu and M. Egashira, "Basic aspects and challenges of semiconductor gas sensors," *MRS Bulletin*, vol. 24, no. 6, pp. 18–24, 1999.

[15] N. Bahlawane, P. A. Premkumar, J. Feldmann, and K. Kohse-Höinghaus, "Preparation of doped spinel cobalt oxide thin films and evaluation of their thermal stability," *Chemical Vapor Deposition*, vol. 13, no. 2-3, pp. 118–122, 2007.

[16] U. S. Choi, G. Sakai, K. Shimanoe, and N. Yamazoe, "Sensing properties of SnO_2-Co_3O_4 composites to CO and H_2," *Sensors and Actuators, B*, vol. 98, no. 2-3, pp. 166–173, 2004.

[17] K. Jayanthi, S. Chawla, K. N. Sood, M. Chhibara, and S. Singh, "Dopant induced morphology changes in ZnO nanocrystals," *Applied Surface Science*, vol. 255, no. 11, pp. 5869–5875, 2009.

[18] B. Chi, H. Lin, and J. Li, "Cations distribution of $Cu_xCo_{3-x}O_4$ and its electrocatalytic activities for oxygen evolution reaction," *International Journal of Hydrogen Energy*, vol. 33, no. 18, pp. 4763–4768, 2008.

[19] R. J. Wu, J. G. Wu, T. K. Tsai, and C. T. Yeh, "Use of cobalt oxide CoOOH in a carbon monoxide sensor operating at low temperatures," *Sensors and Actuators, B*, vol. 120, no. 1, pp. 104–109, 2006.

[20] J. R. Tobias Johnsson Wass, I. Panas, J. Ásbjörnsson, and E. Ahlberg, "Quantum chemical modelling of oxygen reduction on cobalt hydroxide and oxyhydroxide," *Journal of Electroanalytical Chemistry*, vol. 599, no. 2, pp. 295–312, 2007.

[21] H. Gong, J. Q. Hu, J. H. Wang, C. H. Ong, and F. R. Zhu, "Nanocrystalline Cu-doped ZnO thin film gas sensor for CO," *Sensors and Actuators, B*, vol. 115, no. 1, pp. 247–251, 2006.

[22] R. J. Wu, W. C. Chang, K. M. Tsai, and J. G. Wu, "The Novel CO sensing material CoOOH-WO_3 with Au and SWCNT performance enhancement," *Sensors and Actuators, B*, vol. 138, no. 1, pp. 35–41, 2009.

[23] S. Zhuiykov, "Carbon monoxide detection at low temperatures by semiconductor sensor with nanostructured Au-doped CoOOH films," *Sensors and Actuators, B*, vol. 129, no. 1, pp. 431–441, 2008.

[24] L. Liu, C. Guo, S. Li, L. Wang, Q. Dong, and W. Li, "Improved H_2 sensing properties of Co-doped SnO_2 nanofibers," *Sensors and Actuators, B*, vol. 150, no. 2, pp. 806–810, 2010.

[25] N. Singh, C. Yan, and P. S. Lee, "Room temperature CO gas sensing using Zn-doped In_2O_3 single nanowire field effect transistors," *Sensors and Actuators, B*, vol. 150, no. 1, pp. 19–24, 2010.

[26] NF X 70-100 French Standard, "Fire Tests: analysis of pyrolysis and combustion gases," ANFOR, pp. 51, 1986.

[27] R. A. Potyrailo, H. Ghiradella, A. Vertiatchikh, K. Dovidenko, J. R. Cournoyer, and E. Olson, "Morpho butterfly wing scales demonstrate highly selective vapour response," *Nature Photonics*, vol. 1, no. 2, pp. 123–128, 2007.